

Received March 9, 2021, accepted March 21, 2021, date of publication March 24, 2021, date of current version April 6, 2021.

Digital Object Identifier 10.1109/ACCESS.2021.3068821

A Comprehensive Disturbing Effect Analysis of Multi-Sectional Rotor Slot Geometry for Induction Machines in Electrical Vehicles

ABDULSAMED LORDOGLU^{1,3}, (Student Member, IEEE),

MEHMET ONUR GULBAHCE², (Member, IEEE),

AND DERYA AHMET KOCABAS³, (Member, IEEE)

¹Department of Electrical Engineering, Yildiz Technical University at Davutpasa, 34220 Istanbul, Turkey

²Department of Electrical and Electronic Engineering, Fatih Sultan Mehmet Vakif University at Halic, 34445 Istanbul, Turkey

³Department of Electrical Engineering, Istanbul Technical University at Maslak, 34467 Istanbul, Turkey

Corresponding author: Mehmet Onur Gulbahce (mogulbahce@fsm.edu.tr)


ABSTRACT Although the performance of an Induction Motor (IM) can be maximized for any speed by use of an inverter, there is still room to contribute by optimizing the rotor slot shape while decreasing the mechanical disturbing effects and acoustic noise. This paper focuses on the effect of different individual rotor slot shapes on the performance of an IM including overall space harmonic, vibration and acoustic effects. A number of rotor slot shapes were implemented to the rotor of a commercial IM and efficiency of all designs were maximized for constant torque region by optimization. Afterwards, operational performance including starting, breakdown and rated operations; moreover, harmonic content and torque ripple were analyzed numerically in association with the mentioned rotor slot shapes. Best performing 4 rotor slot shapes in terms of chosen operational quantities were designated. Furthermore, the determined motors were carried out to vibration and acoustic noise analysis. Superposed acoustic disturbances in terms of sound power level for different harmonic frequencies were obtained and results are given in comparison. All-in-all, this paper contributes to associating the end-to-end disturbing effects to certain rotor slot shapes. This study determines disturbance and performance criteria for choosing an appropriate motor for an IM to be used in an electric vehicle. It was shown that rotor slot shape still deserves considerable attention to increase the performance of an IM while decreasing the adverse effects of space harmonics, mechanical vibration and acoustic disturbance.

INDEX TERMS Induction motor, rotor slot shape, acoustics analysis, mechanical vibration, acoustic noise, space harmonic.

I. INTRODUCTION

Environmental pollution, global warming, depletion of fossil fuels and energy efficiency have increased interest in electric vehicles because of their low fuel consumption and low cost, quiet operation and low maintenance costs. Increasing interest in electric vehicles has also increased efforts to develop better electric propulsion motors, which is the most important component in electric vehicles [1].

Machines designed to meet the desired performance and reliability requirements for electric vehicles must have features such as high torque/power density, wide speed range, overload capacity, high efficiency at all speeds, quick acceleration/deceleration, low cost/weight, durability

The associate editor coordinating the review of this manuscript and approving it for publication was Qiuye Sun .

in harsh environmental conditions, long life and low vibration/noise. The main types of electrical machines used in electric vehicles are direct current motor (DC), caged rotor induction motor (CRIM), permanent magnet synchronous motor (PMSM), switched reluctance motor (SRM) and synchronous reluctance (SynRM) motor. Cons and pros of these motors according to some operational criteria are shown in the Table 1 and it can be seen that CRIM serves low cost, simplicity and robustness, high efficiency, low vibration/noise with high performance compared to other motors [2], [3].

CRIM having rotor slots with low skin effect have both low starting torque and high efficiency, while the ones with high skin effect have both high starting torque and low efficiency. However, to combine high starting torque and low starting current with low rated slip and high efficiency, it is possible to obtain a naturally varying rotor resistance by changing

TABLE 1. Comparison of electric machines used in electric vehicle applications (where '+' denotes advantages, '-' disadvantages, '0' neutral rating) [3].

| Criteria | Types of Machines | | | | |
|-------------------------------|-------------------|------|------|-----|-------|
| | DC | CRIM | PMSM | SRM | SynRM |
| Torque/power density | - | 0 | ++ | 0 | 0 |
| Overload capability | - | + | + | + | ++ |
| Efficiency | - | + | ++ | + | + |
| Cost | 0 | ++ | - | + | ++ |
| Simplicity/manufacturability | ++ | ++ | 0 | ++ | ++ |
| Robustness | 0 | ++ | + | ++ | ++ |
| Noise/vibration/torque ripple | - | ++ | ++ | - | - |
| Potential | - | ++ | ++ | ++ | + |
| Controllability | ++ | + | + | 0 | + |
| Reliability | - | ++ | + | ++ | ++ |
| Size/weight/volume | - | + | ++ | + | + |
| Lifetime | - | ++ | + | ++ | ++ |

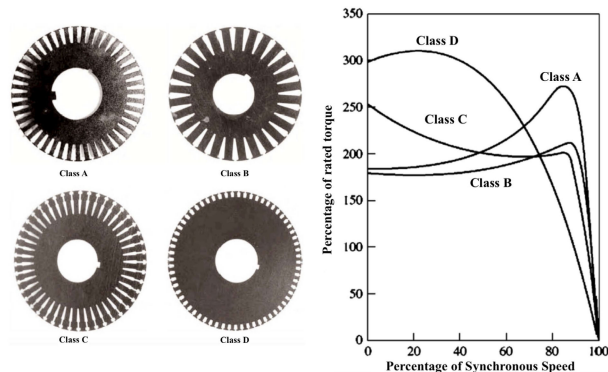


FIGURE 1. Rotor slot shapes and speed-torque curves of NEMA classes [5].

the shape and dimensions of rotor slot while implementing deep-slots and double-cage structures are also possible [4]. Large bar resistance at low speeds helps in increasing the starting torque, while large resistance at higher speed decreases the efficiency. Leakage reactance is increased by higher rotor frequencies and naturally it is reduced by decreasing slip. All directly affect the electrical, magnetic, mechanical and acoustic performance of the CRIM [5].

In [6], shorter and wider rotor slots are recommended for better starting torque and power factor, while deeper and wider rotor slots are for better efficiency. According to [7], the round rotor slot has 4.8% lower vibration than that of the rectangular rotor slot. In [8], [9], optimal rotor slot size is determined by using various optimization methods. The objective of these studies is to obtain a rotor slot geometry in which maximum motor efficiency is achieved. In some studies where different rotor slot shapes were compared, the rotor slot area was kept constant, however rotor slot area was shown to be effective on machine performance in studies that make a single type of rotor optimization [10], [11], [37].

A wide variety of speed-torque curves can be obtained by varying rotor structure. NEMA has defined standard design series with different speed-torque curves to assist the industry in selecting the proper motor for a variety of applications [5]. Fig. 1 shows typical rotor slot shapes and speed-torque curves for the four standard NEMA design classes. The rotor slots in class A are large while the ones in B are large and deep. Double-cage rotor is used for class C whilst small rotor slots are implemented for class D. Some researchers designed rotor slot types of NEMA classes and made comparative analysis [12]–[14]. In [14] A, B, C, D type rotors having same rotor slot area in order to keep the cost constant were designed and were examined in terms of performance. It is concluded that double cage motors are better for both starting and rated operation.

Air-gap magnetomotive force (MMF) waveform, directly affects operating performance of CRIM related to its harmonic content. MMF shape is based on the multiplication of conductor distribution and time-varying current. Depending on the tooth and slot distribution, MMF is in stepped-shape serving unavoidable space harmonics to rotor although the

motor is fed by pure sinusoidal voltage. By Fourier analysis, harmonic spectrum can be calculated. If the motor is supplied by an inverter, a collision between time and space harmonics occur. Space harmonics are known to have negative effects on machine performance by generating vibration and noise, reducing torque at rated speed, creating additional losses and bringing about thermal stress. Effects of space harmonics can only be reduced by making changes to windings and core of the motor both on stator and rotor. In previous studies, methods using different winding connections in the same stator core were presented [15]–[17] while others use non-uniform slot and conductor distribution in different ways [18], [19]. Also, rotor space harmonic effects are analyzed by other authors by changing rotor slot shape and dimensions [20].

Vibration and noise including the effect of space harmonics can be classified into three main classes as aerodynamic, mechanical and electromagnetic. Mechanical noise is created by mechanical factors such as bearings. The frequency of the generated noise is relatively low and therefore easy to distinguish from other noise components. Aerodynamic noise is generated by bodies interacting with air such as cooling fan or slot openings. Electromagnetic noise is associated with space and time harmonics, magnetic saturation, phase unbalance and also reluctance change according to stator and rotor slot openings and geometry [21].

Electromagnetic noise is formed by radial forces created by air-gap mmf causing the stator vibrate. The vibrating stator contacts the air and causes noise to spread from the stator surface which can be calculated analytically [22]–[25], [38]. These studies include optimisation of main dimensions, presentation of designs for different numbers of rotor types, evaluation of operational quantities for determining the electromagnetic noise without classification.

In this study, different CRIMs were analyzed in terms of both electromagnetic and mechanical operational performance, space harmonic and adverse magnetic noise effects to serve a better performance to an electric vehicle. A number of CRIMs having same stator core and winding, but rotors serving different rotor slot shapes and geometries were analyzed and the results are presented. Existing and newly created slot shapes in different dimensions were implemented to the same

TABLE 2. Motor design parameters and final design dimensions.

| Parameter | Value | Unit | Parameter | Value | Unit |
|------------------|-------|------|------------------------|-------|------|
| Power | 104 | kW | Number of stator slots | 60 | - |
| Max. Power | 125 | kW | Number of rotor slots | 74 | - |
| Voltage | 220 | V | Stator outer diameter | 281 | mm |
| Rated speed | 4000 | rpm | Stator inner diameter | 178 | mm |
| Max. Speed | 11400 | rpm | Rotor outer diameter | 176.6 | mm |
| Rated torque | 250 | Nm | Rotor inner diameter | 90 | mm |
| Max. Torque | 300 | Nm | Length | 154 | mm |
| Supply frequency | 133 | Hz | Air gap | 0.7 | mm |

TABLE 3. Magnetic constraints of induction machine parts [26].

| Induction Machine Parts | Flux Density (T) |
|-------------------------|------------------|
| Air gap | 0.7-0.9 |
| Stator yoke | 1.4-2.0 |
| Stator tooth | 1.4-2.1 |
| Rotor tooth | 1.5-2.2 |
| Rotor yoke | 1.0-1.9 |

rotor and 13 motors with different rotor slots were designed under certain classification. The numerical analysis was performed at constant torque region by 2D Transient FEM. The results were exported to deformation and acoustic toolboxes. Results including torque-speed curves, air-gap flux density distribution, harmonic spectrum, torque ripple, mechanical stress and acoustic noise are given in comparison.

II. INDUCTION MOTOR DESIGN FOR ELECTRIC VEHICLE APPLICATIONS

The design requirements for motors used in electric vehicles are motor power, number of poles, stator and rotor slot numbers, speed and acceleration ranges. The values for the motor to be analyzed were determined from those features used in practical applications. The chosen motor design criteria are given in Table 2. The data in Table 2 is derived from commercial EV traction motors (BMW i3 and Tesla S) [36].

In order to ensure unsaturated operation with a low level of core loss to contribute to a higher efficiency, the magnetic constraints shown in Table 3 were specified for various parts of the motor to be analyzed [26].

Calculated physical dimensions of the machine via conventional analytical methods were implemented into a FEA software and those values were optimized by FEA considering all mentioned constraints and the final main dimensions and numerical values were determined from the results as shown in Table 2.

In this study, coupled circuit two-dimensional (2D) transient magnetic model is used for FEA to optimize and design. All simulations were performed with Ansys Electronics Desktop which uses the actual B-H curve of magnetic material that reflects saturation effects. Besides, skin effect in rotor bar and motion of the rotor with respect to stator were also considered. During FEA process, magnetic field was taken to be parallel to center lines of the poles corresponding Neumann boundary conditions. Besides, no flux passes throughout the outer surface of the stator. By this, it was ensured that vector potential on stator boundary has a constant value satisfying the Dirichlet's boundary condition.

Previous studies proved that skewing the rotor slots contributes in cancelling the adverse effect of space harmonics and one rotor slot skewing was shown to be a proper solution [26]. In this study, one slot skewing was applied to all rotor designs.

Electrical and magnetic performances of a motor are directly related to stator and rotor slot geometries. The change in rotor slot geometry of CRIM directly affects the change in rotor resistance, leakage inductance and space harmonic distribution. This change has a direct effect on all operational quantities and rated values including stator current, torque and shaft power. For a better comparison of the effect of change in rotor slot geometry, no change in stator slots were made and rotor main geometrical dimensions are kept constant. A double-layer winding with two parallel branches having 12 conductors per slot was implemented to the stator slots. Stator slot design providing a constant tooth width was chosen and M19-29G material was used in stator and rotor cores. Aluminium was used for rotor bars. For a better examination of space harmonics effects, mesh structure was preferred to be overly dense in return for time consuming analysis.

A. CALCULATION OF ROTOR SLOT PROPERTIES

Rotor slot shapes used in commercial CRIMs have different types of shape. For the sake of the study, rotor slot geometries used in this study were inspired from those used in commercial ones and 13 different rotor slot geometries were created mainly in three classes which are rectangular, oval and trapezoidal. All mentioned three classes consist of deep slots and multiple cage with expanding or narrowing slots towards rotor shaft. In addition, all 13 rotors have closed slot openings to reduce parasitic torque and noise. The designed rotor slot geometries are shown in Fig. 2.

In previous studies, rotor slot areas were mostly kept constant to compare the effect of different rotor slot geometries over the performance of the motors [7], [11], [27], [28]. However, in studies analysing and optimising the effect of single rotor slot shape, rotor slot area is mentioned to be highly effective on the performance of a CRIM [9], [13], [29]. Therefore, keeping rotor slot area constant at a certain value for all rotor types can provide a good performance for some rotor slot types while others show poor performance in terms of operational performance parameters such as starting current, starting torque, power factor and efficiency. Since the focus of this study is the best performance, authors preferred not to keep the rotor slot area constant.

Rotor slot dimensions for each slot shape were optimized to provide the best efficiency among constant torque region while considering the magnetic limits specified in Table 3. A commercial magnetic analysis software was used for the optimisation to choose the best dimension for each slot shape given in Fig. 2. For a better comparison, values given in Table 4-8 are normalised according to that of $\phi 1$ rotor slot type and its value is inserted as **1 pu** to the tables.

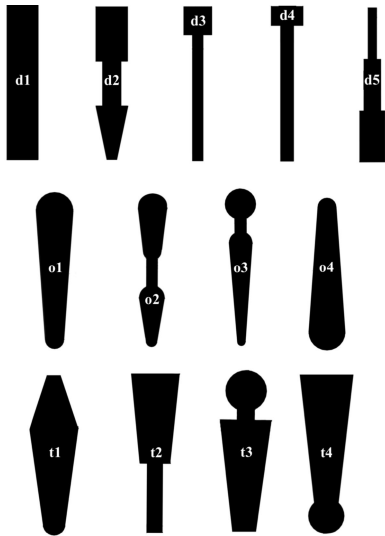


FIGURE 2. Rotor slot shapes of designed motors.

TABLE 4. Rotor slot areas of designed motors.

| Types of designed motors | Rotor slot areas (pu) |
|--------------------------|-----------------------|
| <i>d4</i> | 0.826 |
| <i>d5</i> | 0.844 |
| <i>t4</i> | 0.849 |
| <i>d3</i> | 0.864 |
| <i>t3</i> | 0.884 |
| <i>d2</i> | 0.894 |
| <i>d1</i> | 0.904 |
| <i>o3</i> | 0.904 |
| <i>t1</i> | 0.904 |
| <i>t2</i> | 0.918 |
| <i>o1</i> | 1.000 |
| <i>o4</i> | 1.000 |
| <i>o2</i> | 1.093 |

Calculated areas for the rotor slot shapes are given in Table 4 after slot area optimisation. It can be seen from the table that oval rotor slot family requires more area to meet the desired magnetic and operational requirements in Table 2 and 3.

III. PERFORMANCE COMPARISON

A. SPEED-TORQUE CHARACTERISTICS

In a conventional CRIM, at rated operation, motor has low resistance and impedance at a relatively low rotor frequency, lower rated slip than that of starting and high efficiency. At starting, resistance is higher related to skin effect, motor impedance and rotor frequency are higher related to higher slip. Therefore, for a motor for uninterrupted operation, rotor has to be designed with a low resistance to ensure a high efficiency while starting torque is low and starting current is high.

For a frequently starting motor, rotor has to be designed with a higher resistance to ensure a low starting current and high starting torque. Related to skin effect, effective rotor slot area changes according to slip although the physical rotor slot area remains the same. The change of rotor slot effective area and leakage flux distributions among rotor slots can be

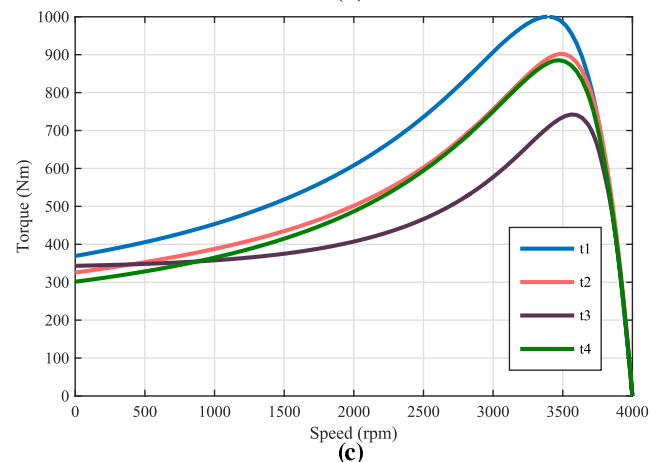
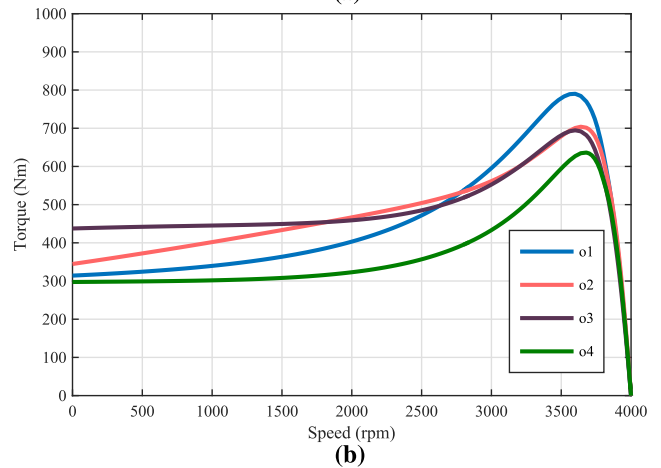
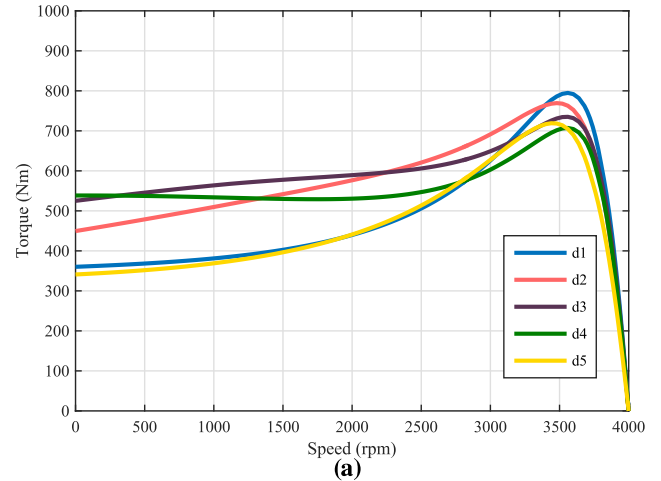


FIGURE 3. Speed-Torque curves of a) *d1, d2, d3, d4, d5*, b) *o1, o2, o3, o4*, c) *t1, t2, t3, t4*.

adjusted by changing the shape and dimensions of the slots and also by injecting multi-material inside the slots. Deep slot design and double cage structures are used to ensure high rotor resistance at start-up and low rotor resistance at rated operation.

A rotor having slots formed by different geometric shapes those placed one on the top of another can be referred as a multi-cage rotor having cages in electrical connection those have a common end-ring.

TABLE 5. Starting characteristics of the designed motors.

| Starting Torque (pu) | | Starting Rotor Resistance (pu) | | Starting Current (pu) | | Starting Rotor Reactance (pu) | |
|----------------------|------|--------------------------------|------|-----------------------|------|-------------------------------|------|
| Descending | | Descending | | Ascending | | Descending | |
| d4 | 1.71 | d4 | 1.73 | o4 | 0.84 | o4 | 1.48 |
| d3 | 1.67 | o3 | 1.52 | d5 | 0.90 | d5 | 1.29 |
| d2 | 1.43 | d3 | 1.43 | t3 | 0.94 | t3 | 1.13 |
| o3 | 1.39 | d5 | 1.38 | o3 | 0.96 | o3 | 1.05 |
| t1 | 1.18 | o4 | 1.37 | d4 | 0.99 | o1 | 1 |
| d1 | 1.15 | t3 | 1.24 | o1 | 1 | d1 | 0.96 |
| o2 | 1.10 | d1 | 1.13 | d1 | 1.01 | o2 | 0.94 |
| t3 | 1.09 | o2 | 1.05 | o2 | 1.02 | d4 | 0.90 |
| d5 | 1.09 | o1 | 1 | d3 | 1.08 | t4 | 0.80 |
| t2 | 1.04 | d2 | 0.99 | t4 | 1.09 | d2 | 0.77 |
| o1 | 1 | t2 | 0.80 | d2 | 1.09 | d3 | 0.74 |
| t4 | 0.96 | t4 | 0.80 | t2 | 1.13 | t2 | 0.72 |
| o4 | 0.95 | t1 | 0.76 | t1 | 1.23 | t1 | 0.53 |

TABLE 6. Maximum and rated torque characteristics of the designed motors.

| Loading Capability (pu) | | Pull Out Slip (pu) | | Pull Out Torque (pu) | | Rotor Reactance at Full Load (pu) | | Rotor Resistance at Full Load (pu) | | Rated Slip (pu) | | Efficiency (pu) | |
|-------------------------|------|--------------------|------|----------------------|------|-----------------------------------|-------|------------------------------------|------|-----------------|------|-----------------|--------|
| Descending | | Descending | | Descending | | Ascending | | Ascending | | Ascending | | Descending | |
| t1 | 1.26 | t1 | 1.49 | t1 | 1.27 | t1 | 0.774 | o2 | 0.93 | o2 | 0.94 | o1 | 1 |
| t2 | 1.14 | d5 | 1.36 | t2 | 1.14 | t2 | 0.854 | o1 | 1 | o1 | 1 | o2 | 1 |
| t4 | 1.12 | t4 | 1.31 | t4 | 1.12 | t4 | 0.879 | o4 | 1.00 | o4 | 1.02 | d2 | 0.9992 |
| d2 | 1.07 | t2 | 1.27 | d2 | 1.07 | d2 | 0.921 | d2 | 1.05 | d2 | 1.05 | d1 | 0.9992 |
| o1 | 1 | d2 | 1.15 | d1 | 1.01 | d1 | 0.992 | d1 | 1.06 | d1 | 1.06 | o4 | 0.9991 |
| d1 | 1 | d1 | 1.07 | o1 | 1 | o1 | 1 | t2 | 1.08 | t2 | 1.07 | t2 | 0.9986 |
| t3 | 0.94 | d4 | 1.04 | t3 | 0.94 | t3 | 1.070 | o3 | 1.08 | o3 | 1.10 | t4 | 0.9984 |
| d3 | 0.93 | t3 | 1.04 | d3 | 0.93 | d3 | 1.077 | d3 | 1.10 | t3 | 1.12 | t1 | 0.9979 |
| d5 | 0.90 | d3 | 1.02 | d5 | 0.91 | d3 | 1.082 | t3 | 1.11 | d3 | 1.12 | o3 | 0.9979 |
| d4 | 0.89 | o1 | 1 | d4 | 0.90 | d4 | 1.125 | t4 | 1.15 | t4 | 1.14 | t3 | 0.9979 |
| o2 | 0.89 | o3 | 0.94 | o2 | 0.89 | o2 | 1.138 | t1 | 1.15 | t1 | 1.14 | d3 | 0.9974 |
| o3 | 0.88 | o2 | 0.82 | o3 | 0.88 | o3 | 1.150 | d4 | 1.17 | d4 | 1.19 | d4 | 0.9968 |
| o4 | 0.80 | o4 | 0.79 | o4 | 0.81 | o4 | 1.276 | d5 | 1.46 | d5 | 1.51 | d5 | 0.9905 |

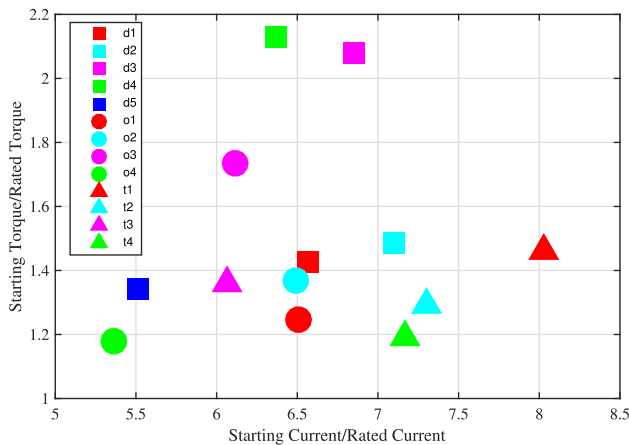


FIGURE 4. Starting characteristics of designed motors.

In this section, torque-speed curves for the motors with the given rotor slot shapes (those grouped in families in previous sections) were obtained and curves for the same slot shape families are compared accordingly. Steady state power and speed values are obtained for a constant torque value for each slot type by 2D transient FEA. The analyzes are repeated for different torque values and integrated torque-speed curves are derived by merging the steady state values for each slot type. Additional operational parameters are extracted from numerical data of an individual analysis. The speed-torque curves for different slot families are shown as subfigures in Fig. 3.

Besides, starting performance comparison for all mentioned motors is given in Fig 4. illustrating the markings those represent the ratios of rated and starting values for current and torque. Calculated characteristic values which are current, torque, resistance and reactance at starting are given in Table 5. Loading capability, pull out slip, pull out torque, rated reactance and resistance, rated slip and efficiency values are shown in the Table 6. All mentioned data were obtained by FEA and represented in *perunit* according to *o1* values.

As seen in Fig. 3, the rotor slot type with the highest starting torque is *d4* with its highest rotor resistance in Table 5. The highest maximum (pull-out) torque belongs to *t1* ensuring the lowest rotor leakage reactance. In detail, *t1* also has the highest pull-out slip ensuring the highest ratio of rotor resistance over rotor leakage reactance. It can be seen in Fig. 4 that the starting current and torque of *o4* (which has the largest starting reactance in Table 5) are both the lowest. Besides, it was seen that rotor slots (*d4*, *d3*, *d2*) having lower ratio of 'upper (cage) area to total slot area' have higher starting torque related to increased skin effect. Fig. 4 can also be used for determining the rotor slot type suitable for the desired starting performance with low current and high torque.

Although it is very well known that starting performance of an IM can be adjusted, here in this study only the effect of rotor slot geometry is analyzed regardless to different control strategies and supply types. All FEA performed under rated voltage and frequency to obtain overall disturbing effect.

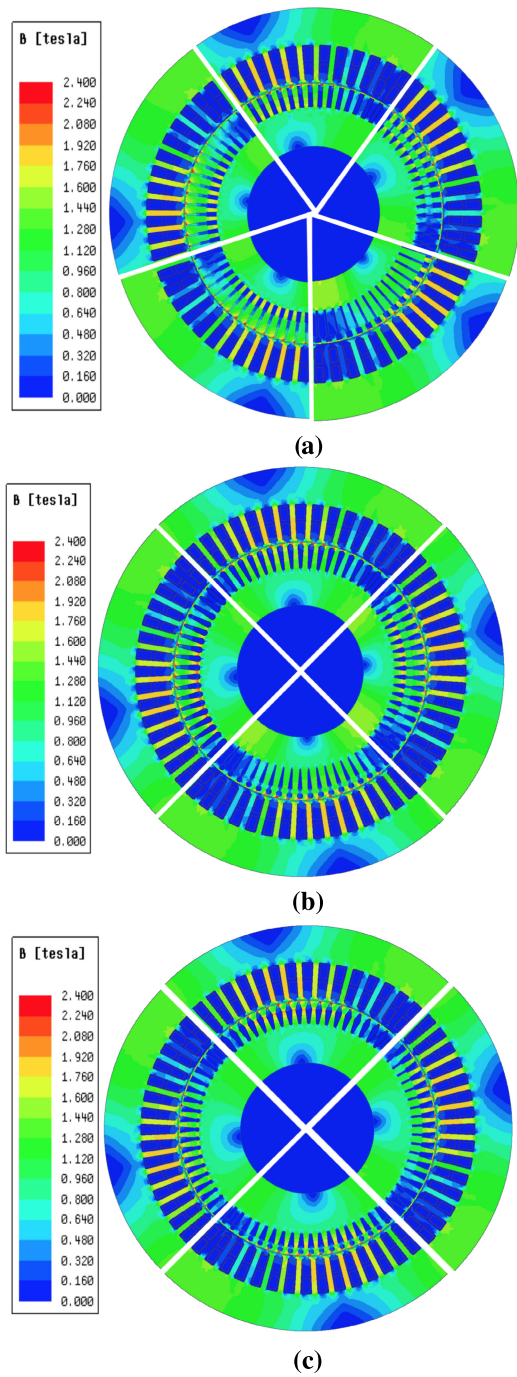


FIGURE 5. Magnetic flux density distributions of a) $d1, d2, d3, d4, d5$, b) $o1, o2, o3, o4$, c) $t1, t2, t3, t4$.

Pull-out torque is an important but not the only criterion in choosing a traction motor for EV applications. All torque values including rated, starting and pull-out are related to rotor circuit parameters directly associated with rotor slot shape and current density distributions. Hence, although the starting performance is controlled by motor drives, the correlation between starting and pull-out torque (also the rated torque) cannot be ignored. The main objective of this study is to compare operational performances of different IMs, not to compare dynamic performances of EVs.

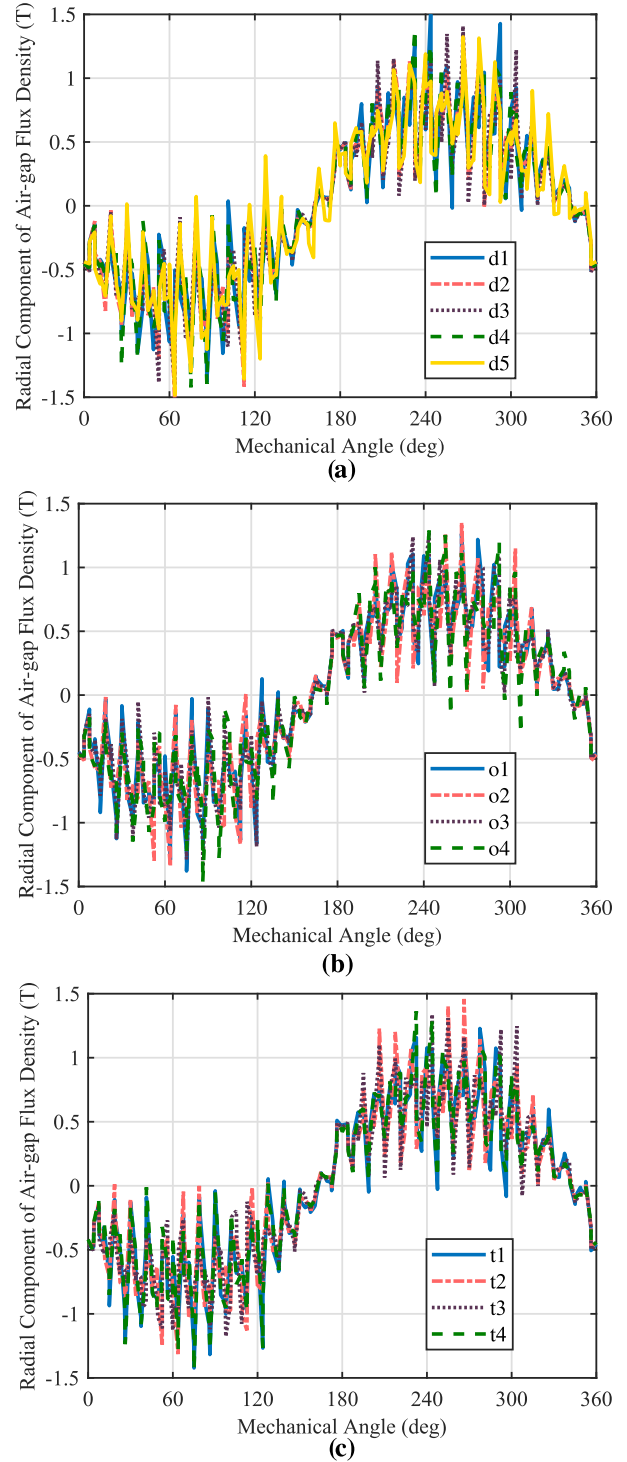


FIGURE 6. The radial component of the air gap magnetic field density waveforms of a) $d1, d2, d3, d4, d5$, b) $o1, o2, o3, o4$, c) $t1, t2, t3, t4$.

Change of rated slip is directly related to rotor resistance as can be seen in Table 6. Table 6 proves that rotor slot types providing higher rotor leakage reactance at full load has a lower maximum torque that is irrelevant to rotor resistance at full load. When it comes to loading capability, the best performance belongs to trapezoidal (t) slot family, whilst oval (o) slot family performance is the worst.

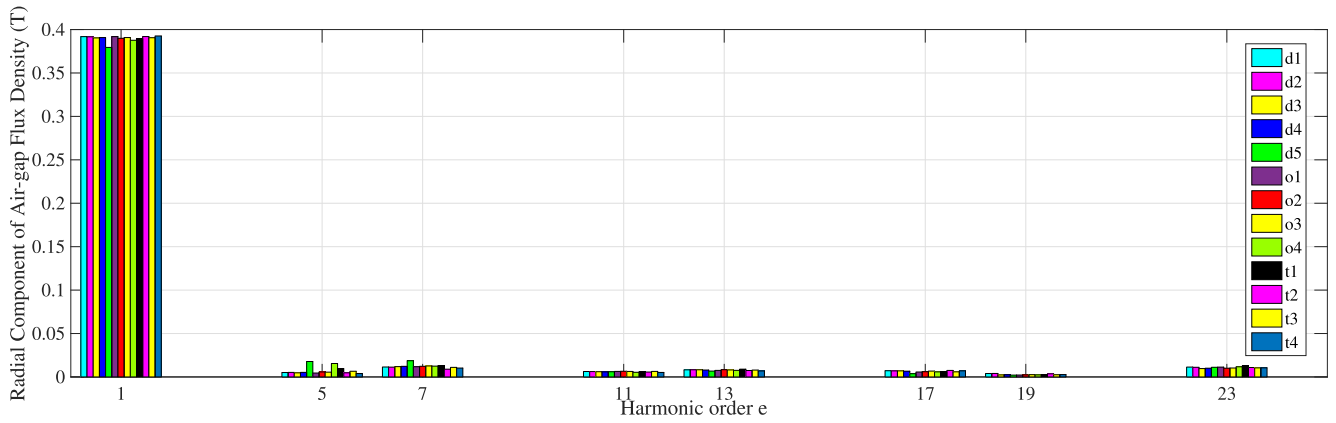


FIGURE 7. Harmonic spectrum of radial component of air gap flux density of designed motors.

B. MAGNETIC PERFORMANCE

Numerous transient magnetic analysis are completed for different slot shapes to obtain torque-speed curves for each. Fig. 5 illustrates the magnetic analysis result samples for all slot shapes grouped in families in sub-figures to provide the reader a good visual comparison. All figures are scaled for the same maximum and minimum values.

C. HARMONIC ANALYSIS

Space harmonics, known as MMF harmonics, have adverse effects on motor performance like noise, vibration and additional losses. Only physical changes in the core and/or winding can possibly eliminate and/or reduce the effects of these harmonics.

Harmonic spectrum contains only odd harmonics related to quarter-wave symmetry. Besides triplen harmonics (order of $3k$) do not generate a rotating field and are insignificant. Thus, only orders of $(6k \pm 1)$ harmonics exist in a symmetrical three phase winding. Harmonics of orders of $(6k + 1)$ rotates in the same direction with the fundamental, while those of order of $(6k - 1)$ rotates in reverse direction [30].

In this study, the radial component of air-gap is extracted by using the embedded calculator of the commercial software. Harmonics of the radial component are calculated by fourier analysis. The change of the radial component of air gap magnetic field density distribution for each slot type was obtained and results grouped in families are given in comparison in Fig. 6. Radial component of air gap flux contains space harmonics created by both stator and rotor. It can be seen from Fig. 6 that motors having different rotor slot shapes have different distributions, although the stator structure is kept unchanged. Harmonic spectrum for each wave in Fig. 6 is given in Fig. 7 in comparison. Harmonic spectrum for slot types are different from each other, although stator contribution is the same for all, while the rotor harmonic contribution is altered according to rotor slot shape.

This is because the change in rotor slots shape directly affects the rotor space harmonic distribution which is added to air gap harmonics. Although the most prominent stator mmf harmonic is the 5th, the order of the most prominent total air gap mmf harmonic can be different related to the effect of

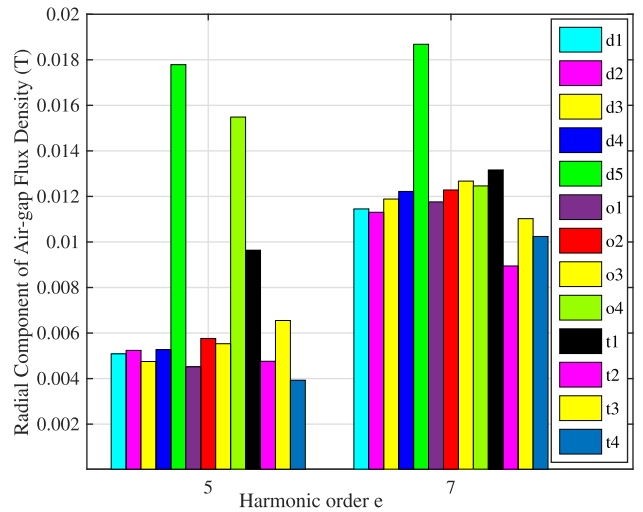


FIGURE 8. 5th and 7th harmonics of radial component of air gap flux density of designed motors.

rotor slot shape as shown in the Fig. 7. 5th and 7th harmonics are given in comparison in Fig. 8.

D. TORQUE RIPPLE ANALYSIS

The steady-state torques including all ripple effects for all slot types are obtained by 2D Transient Magnetic FEA Model. The changes of torques according to mechanical rotation angle of rotor are shown in Fig. 9 as a function of different rotor slot types.

By means of obtained results from numerous transient magnetic analysis, form factors (FF) and ripple factors (RF) of steady-state rated torques for all motors are calculated by (1) and (2). Calculated ripple factors for all motors are given in Table 7. All given data in Table 7 were represented in per unit with reference to $o1$.

$$FF_{Torque} = \frac{Torque_{(RMS)}}{Torque_{(AVG)}} \tag{1}$$

$$RF_{Torque} = \sqrt{FF_{Torque}^2 - 1} \tag{2}$$

As seen in Table 7, the lowest ripple factor belongs to $o4$, the highest to $t4$. Torque ripple is an important but not the only criterion in choosing a traction motor for EV applications.

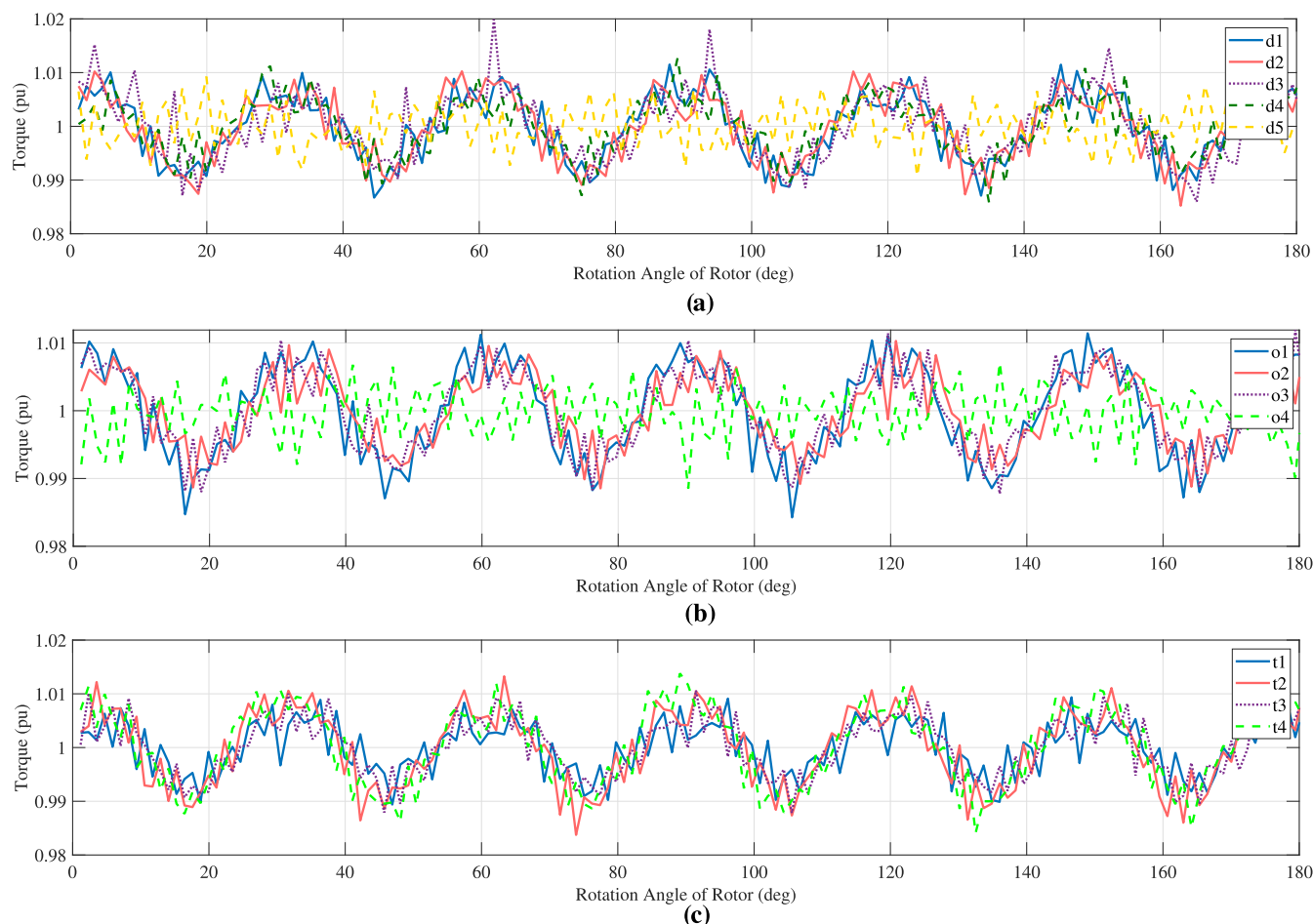


FIGURE 9. Torque as a function of rotation angle for different rotor slot types a) *d1, d2, d3, d4, d5*, b) *o1, o2, o3, o4*, c) *t1, t2, t3, t4*.

TABLE 7. Ripple factors of all designed motors.

| Types of designed motors | Ripple Factors (pu) |
|--------------------------|---------------------|
| <i>o4</i> | 0.545 |
| <i>d5</i> | 0.623 |
| <i>t1</i> | 0.746 |
| <i>o2</i> | 0.777 |
| <i>t3</i> | 0.794 |
| <i>d4</i> | 0.818 |
| <i>o3</i> | 0.837 |
| <i>d3</i> | 0.89 |
| <i>d2</i> | 0.902 |
| <i>d1</i> | 0.912 |
| <i>o1</i> | 1.000 |
| <i>t2</i> | 1.023 |
| <i>t4</i> | 1.049 |

Further investigation is needed for overall operational performance considering “pull-out torque, load capability, starting performance, efficiency, harmonic content, motor vibration and noise”. Although *o4* has a good performance in terms of ripple factor, it is not a good candidate in terms of other operational parameters.

E. VIBRATION AND ACOUSTIC ANALYSIS

Radial forces on the surface of the stator tooth due to the air gap magnetic field density are the main cause of electromagnetic induced vibration and noise and can be analytically

calculated by Maxwell’s stress method [31]. Force density of different harmonics can be evaluated as a function of position (θ) and time (t) by using superposition principle as in (3) where P_n is normal electromagnetic force density, P_e , amplitude of the electromagnetic force of e th harmonic, w_e , angular frequency and ϕ_e , phase angle [31].

$$P_n(\theta, t) = \sum_{e=1}^n P_e \cdot \cos(w_e t - e\theta + \phi_e) \tag{3}$$

The process of creating acoustic noise in electromechanical energy conversion systems is shown in the Fig. 10. Mechanical structure is stimulated by electromagnetic harmonic forces to create acoustic noise. Current passing through slots interacts with air gap magnetic field harmonics that results in high frequency forces acting on stator core. Mechanical vibration within respective frequency range is caused by these harmonic forces that stimulate stator core. Forces created on different parts of stator core have changing directions and magnitudes causing vibration. Resulting vibration at any point causes a displacement at that part of stator core (especially at teeth). The direction of displacement is related to interaction between the instantaneous values of both harmonic flux and current that corresponds to harmonic force frequencies.

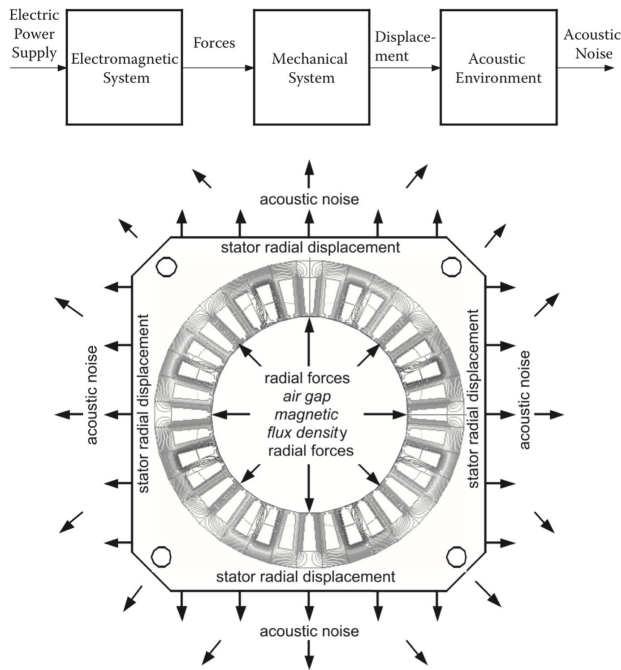


FIGURE 10. The process of creating acoustic noise in electromechanical energy conversion systems [21].

Consequently, interplay between vibrating stator core parts and air causes acoustic noise [21], [32], [33], [34].

Three methods which are Sound Pressure, Sound Power and Sound Intensity are used to measure the sound amplitude. Since sound power definition represents only the power of sound source in dB regardless to distance, this method was used for comparison.

Acoustic analysis was performed for the most prominent harmonics (5th and 7th) which have the greatest disturbance. Only 4 motors were chosen for acoustic analysis which are *o1* as the reference motor, *t4* with the least harmonic content, *d5* with the most harmonic content and *d4* with the most appropriate operational performance considering “starting current, starting torque, efficiency, harmonic content and torque vibration”.

The magnetic results of these 4 motors were transferred to acoustic toolbox of FEA program and the magnetic acoustic noise generated by space harmonics was calculated. First of all, the deformation of the motors were obtained by 2D transient magnetic analysis results. Afterwards, the noise emitted from the stator core for each of 4 motors was computed using the deformation results. Deformation and acoustic analyzes were performed from 0 Hz to 5000 Hz with regards to the sensitive of human ear between 1000 and 4000 Hz. Sample results for deformation at the X-axis are given for 1000 Hz in comparison in Fig. 11. In the figures, it was seen that the deformation is more in the stator slots than in the stator yoke.

Fig. 12 illustrates the sound power level spectra for sample motors in comparison. Although the sound analysis was performed for sound power level, to convert the results into telephone influence factor (TIF) which represents the sensitivity of human ear is more useful for a better interpretation. TIF

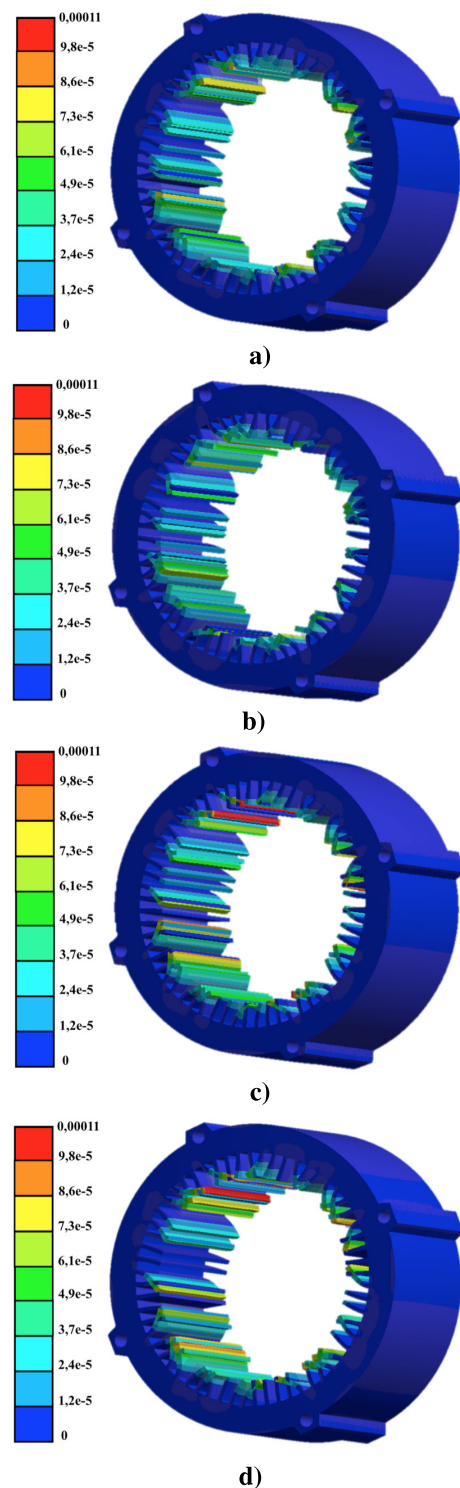


FIGURE 11. Sample deformation results at 1000 Hz for a) *d4*, b) *d5*, c) *t4*, d) *o1*.

which is obtained by physiological and audio tests determines the influence of power systems harmonics on telecommunication systems. It is a modified THD in which the root of the sum of the squares is weighted using factors (weights) that reflect the response of the human ear in (4) where w_i is the TIF weighting factor of i^{th} harmonic, $K^{(i)}$, sound magnitude

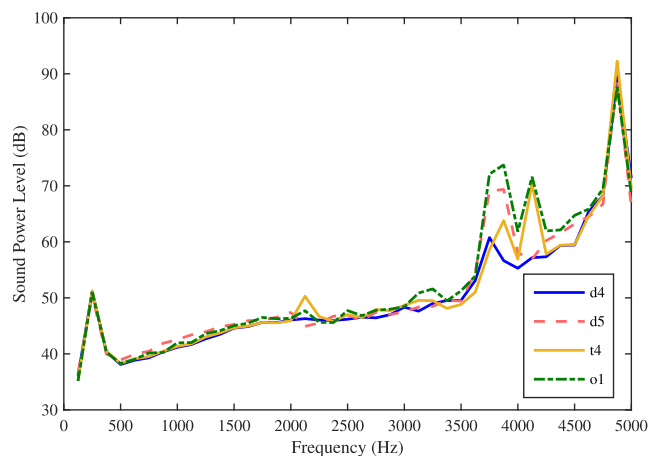


FIGURE 12. Sound power level spectra of d4, d5, t4, o1.

TABLE 8. TIF values of d4, d5, t4 and o1.

| Types of designed motors | TIF (pu) |
|--------------------------|----------|
| d4 | 0.9978 |
| d5 | 1.0031 |
| t4 | 0.98861 |
| o1 | 1 |

to be calculated as weighted.

$$TIF = \frac{\sqrt{\sum_{i=1}^{\infty} (w_i K^{(i)})^2}}{\sqrt{\sum_{i=1}^{\infty} (K^{(i)})^2}} \quad (4)$$

Calculated TIF values using sound power spectra are shown in the Table 8 in per units referenced to o1. It can be seen that the best acoustic performance belongs to t4 rotor slot type.

IV. CONCLUSION

This paper focuses on the effect of different rotor slot shapes on motor performance together with space harmonic, vibration and acoustic effects. Same structure and winding scheme is used for stator core and 13 different rotor slot shapes grouped in 3 families were implemented to rotor to obtain performance change where standard rotor slot shape (o1) performance was accepted as reference. Starting, pull-out and rated operation and effects of rotor resistance, rotor leakage reactance were analyzed and results were represented in comparison.

Since the aim of the study is to obtain the best performance for each rotor slot shape, firstly rotor slot area for each shape was optimized parametrically. All motors were analyzed under constant torque constraint.

Best average starting performance belonged to rectangular slot family followed by oval and trapezoidal ones. Narrowed slots towards centre provided better starting torque than enlarging ones. Best average starting current performance represented by oval family while trapezoidal slots performed the worst.

Highest efficiency belongs to oval, trapezoidal and rectangular families, respectively. The order of the loading capability calculated by “pull-out torque/rated torque” was shown to be as trapezoidal, rectangular and oval.

In terms of space harmonic effect, especially belonging to 5th and 7th, the least harmonic content belongs to t4 while the highest belongs to d5. d4 was shown to exhibit the most appropriate operational performance considering “starting current, starting torque, efficiency, harmonic content and torque vibration”.

Torque ripples (by itself, which is an important but not the only criterion in choosing a traction motor for EV applications) were also compared and o4 was shown to be the best, while it has one of the worst performances among all.

Moreover, acoustic analysis for 4 chosen motors were performed and results were shown to be in harmony with the harmonic analysis results.

This study is mainly a multi-case study and the main contribution of the authors and the study is to present overall disturbing effects analysis associating rotor slot design to acoustic effect. The manuscript includes analyzes for innovative and previously unused multi-sectional rotor slot designs together with several well-known ones associating all space harmonic, torque ripple, vibration and acoustic disturbances to each other for all those given individual slot designs.

All-in-all, in this paper, disturbance and performance criterions for choosing an appropriate motor accommodating a certain rotor slot shape for an electric vehicle were investigated and it was shown that rotor slot shape deserves considerable attention in choosing and increasing the performance of the induction motor while decreasing and/or optimizing the adverse effects of space harmonics, mechanical vibration and acoustic disturbances.

As a future study, the authors aim to optimize each geometric parameter of the rotor slot shapes with meta-heuristic algorithms. It is possible to used different methods for this purpose to have result in comparison.

REFERENCES

- [1] S. Leitman and B. Brant, *Build Your Own Electric Vehicle*. New York, NY, USA: McGraw-Hill, 2013.
- [2] T. Finken, M. Felden, and K. Hameyer, “Comparison and design of different electrical machine types regarding their applicability in hybrid electrical vehicles,” in *Proc. 18th Int. Conf. Electr. Mach.*, Sep. 2008, pp. 1–5.
- [3] M. Yilmaz, “Limitations/capabilities of electric machine technologies and modeling approaches for electric motor design and analysis in plug-in electric vehicle applications,” *Renew. Sustain. Energy Rev.*, vol. 52, pp. 80–99, Dec. 2015.
- [4] A. E. Fitzgerald, C. Kingsley, S. D. Umans, and B. James, *Electric Machinery*. New York, NY, USA: McGraw-Hill, 2003.
- [5] S. J. Chapman, *Electric Machinery Fundamentals*. New York, NY, USA: McGraw-Hill, 2012.
- [6] M. Junaid Akhtar, R. K. Behera, and S. K. Parida, “Optimized rotor slot shape for squirrel cage induction motor in electric propulsion application,” in *Proc. IEEE 6th India Int. Conf. Power Electron. (IICPE)*, Kurukshestra, India, Dec. 2014, pp. 3–7.
- [7] P. Pao-La-Or, S. Peaiyoung, T. Kulworawanichpong, and S. Sujitjorn, “Effects of the geometry of the rotor slots on the mechanical vibration of three-phase induction motors,” in *Proc. 7th WSEAS Int. Conf. Simulation, Modelling Optim.*, Beijing, China, Sep. 2007, pp. 434–438.
- [8] B. Yenipinar, C. Yilmaz, and Y. M. F. Sonmez ve Işık, “Optimizing the rotor slot dimensions of asynchronous motor using different optimization methods and investigating effects on the motor performance,” *J. Polytechnic*, vol. 21, no. 1, pp. 1–6, 2018.

- [9] G. Lee, S. Min, and J.-P. Hong, "Optimal shape design of rotor slot in squirrel-cage induction motor considering torque characteristics," *IEEE Trans. Magn.*, vol. 49, no. 5, pp. 2197–2200, May 2013.
- [10] E. Ünlükaya, A. G. Yetgin, and A. M. Çanaköğlü ve Turan, "Rotor oluk şekillerinin asenkron motor performansına etkileri," in *Proc. Elektrik-Elektronik-Bilgisayar Biyomedika Mühendisliği Semp.*, Bursa, Turkey, Dec. 2014, pp. 27–29.
- [11] S. Sal and L. T. Ergene, "Analysis of the rotor bar geometry's effect on the induction motor performance with finite element method," in *Proc. Nat. Conf. Electr., Electron. Comput. Eng.*, Bursa, Turkey, Dec. 2010, pp. 320–324.
- [12] K. I. Nikolaou, M. E. Beniakar, and A. G. Kladis, "Design considerations in induction motors for ship thruster propulsion," in *Proc. Int. Conf. Electr. Mach. (ICEM)*, Berlin, Germany, Sep. 2014, pp. 2286–2292.
- [13] D. Zhang, C. S. Park, and C. S. Koh, "A new optimal design method of rotor slot of three-phase squirrel cage induction motor for NEMA class d speed-torque characteristic using multi-objective optimization algorithm," *IEEE Trans. Magn.*, vol. 48, no. 2, pp. 879–882, Feb. 2012.
- [14] S. Sal, M. Imeryuz, and L. T. Ergene, "The analysis of the squirrel cage induction motor rotor bars under the cost constraint," *EMO Bilimsel Dergi*, vol. 2, no. 3, pp. 23–28, 2012.
- [15] A. Hughes, "New 3-phase winding of low MMF-harmonic content," *Proc. Inst. Electr. Eng.*, vol. 117, no. 8, pp. 1657–1666, 1970.
- [16] M. Centner and R. Hanitsch, "Fractional slot-winding with asymmetrical stator slot-layout," in *Proc. Int. Symp. Power Electron., Electr. Drives, Autom. Motion*, Taormina, Italy, May 2006, pp. 108–110.
- [17] H. Asgharpour-Alamdari, Y. Alinejad-Beromi, and H. Yaghibi, "Improvement of induction motor operation using a new winding scheme for reduction of the magnetomotive force distortion," *IET Electr. Power Appl.*, vol. 12, no. 3, pp. 323–331, Mar. 2018.
- [18] D. A. Kocabas and A. F. Mergen, "Performance and magnetic analysis of the novel stator structure compared with a standard induction machine," in *Proc. IEEE Int. Symp. Ind. Electron.*, Cambridge, U.K., Jun. 2008, pp. 686–691.
- [19] D. A. Kocabas, "Space harmonic effect comparison between a standard induction motor and a motor with a novel winding arrangement," in *Proc. IEEE Int. Electric Mach. Drives Conf.*, Miami, FL, USA, May 2009, pp. 65–69.
- [20] N. F. Serteller, "Contribution to the reduction of time harmonic effects in caged induction machines with slot design," Ph.D. dissertation, Fac. Eng., Marmara Univ., Istanbul, Turkey, 2000.
- [21] J. F. Gieras, C. Wang, and J. C. Lai, *Noise of Polyphase Electric Motors*. Boca Raton, FL, USA: CRC Press, 2005.
- [22] B. Weilharter, "Noise computation of induction machines," Ph.D. dissertation, Fac. Elect. Inf. Eng., Graz Univ. Technol., Graz, Austria, 2012.
- [23] M. K. R. Nguyen Haettel and A. Daneryd, "Prediction of noise generated by electromagnetic forces in induction motors," in *Proc. COMSOL Conf.*, Cambridge, U.K., 2014, pp. 1–5.
- [24] K. C. Maliti, "Modeling and analysis of magnetic noise in squirrel-cage induction motors," Ph.D. dissertation, Royal Inst. Technol., Stockholm, Sweden, 2000.
- [25] M. K. Nguyen, "Predicting electromagnetic noise in induction motors," M.S. thesis, Roy. Inst. Technol., Stockholm, Sweden, 2014.
- [26] J. Pyrhonen and T. V. Jokinen ve Hrabovcova, *Design of Rotating Electrical Machines*. Hoboken, NJ, USA: Wiley, 2013.
- [27] O. A. Turcanu, T. Tudorache, and V. Fireteanu, "Influence of squirrel-cage bar cross-section geometry on induction motor performances," in *Proc. Int. Symp. Power Electron., Electr. Drives, Autom. Motion*, Taormina, Italy, 2006, pp. 1438–1443.
- [28] V. Fireteanu, T. Tudorache, and O. A. Turcanu, "Optimal design of rotor slot geometry of squirrel-cage type induction motors," in *Proc. IEEE Int. Electric Mach. Drives Conf.*, Antalya, Turkey, May 2007, pp. 537–542.
- [29] M. R. Feyzi and H. V. Kalankesh, "Optimization of induction motor design by using the finite element method," in *Proc. Can. Conf. Electr. Comput. Eng.*, Toronto, ON, Canada, 2001, pp. 845–850.
- [30] M. O. Gulbahce and D. A. Kocabas, "High-speed solid rotor induction motor design with improved efficiency and decreased harmonic effect," *IET Electric Power Appl.*, vol. 12, no. 8, pp. 1126–1133, Sep. 2018.
- [31] W. Deng and S. Zuo, "Electromagnetic vibration and noise of the permanent-magnet synchronous motors for electric vehicles: An overview," *IEEE Trans. Transport. Electric.*, vol. 5, no. 1, pp. 59–70, Mar. 2019.
- [32] S. L. Nau and H. G. G. Mello, "Acoustic noise in induction motors: Causes and solutions," in *Proc. 47th Annu. Conf. Petroleum Chem. Ind. Tech. Conf.*, San Antonio, TX, USA, 2000, pp. 253–263.
- [33] I. Boldea and S. A. ve Nasar, *The Induction Machine Handbook*. Boca Raton, FL, USA: CRC Press, 2002.
- [34] R. S. Curiaac and S. Singhal, "Magnetic noise in induction motors," in *Proc. Noise Control Acoustics Division Conf.*, Dearborn, MI, USA, Jul. 2008, pp. 243–247.
- [35] E. Fuchs and M. Mohammad, *Power Quality in Power Systems and Electrical Machines*. New York, NY, USA: Academic, 2015.
- [36] D. Staton and J. Goss, "Open source electric motor models for commercial EV & hybrid traction motors," CWIEME, Berlin, Germany, Tech. Rep. 64747945, Jun. 2017.
- [37] H. J. Lee, S. H. Im, and D. Y. G. S. Um Park, "A design of rotor bar for improving starting torque by analyzing rotor resistance and reactance in squirrel cage induction motor," *IEEE Trans. Magn.*, vol. 54, no. 3, Mar. 2018, Art. no. 8201404.
- [38] M. A. Khan, F. Khan, L. U. Rahman, and A. Fatima, "Analysis and electromagnetic noise suppression of three-phase squirrel cage induction motor," in *Proc. Int. Conf. Comput., Electron. Electr. Eng. (ICE Cube)*, Quetta, Pakistan, Nov. 2018, pp. 1–5.



ABDULSAMED LORDOGLU (Student Member, IEEE) received the B.S. degree in electrical engineering from Yildiz Technical University, Istanbul, Turkey, in 2016, and the M.Sc. degree from the Electrical Engineering Program, Institute of Science and Technology, ITU, in 2019, where he is currently pursuing the Ph.D. degree. He has been a Research Assistant with the Department of Electrical Engineering, Electrics and Electronics Faculty, YTU, since 2017. His main research interests

include design and optimization of electrical machines, harmonics and acoustic noise in electrical machines, power electronics, and electric and hybrid electric vehicles.



MEHMET ONUR GULBAHCE (Member, IEEE) received the B.S. degree in electrical engineering from Istanbul University, Istanbul, Turkey, in 2010, and the M.Sc. and Ph.D. degrees from the Electrical Engineering Program, Institute of Science and Technology, ITU, in 2013 and 2019, respectively. He was also a Research Assistant with the Department of Electrical Engineering, ITU, from 2011 to 2019. Since September 2019, he has been an Assistant Professor with the Department of Electrical and Electronics Engineering, Fatih Sultan Mehmet Vakif University. His main research interests include design and optimization of high-speed electrical machines, harmonics in electrical machines, electrical drives, and compact and efficient converter systems.



DERYA AHMET KOCABAS (Member, IEEE) received the B.S. degree in electrical engineering from ITU, Istanbul, Turkey, in 1994, and the M.Sc. and Ph.D. degrees from the Electrical Engineering Program, Institute of Science and Technology, ITU, in 1997 and 2004, respectively. His main subjects of concern are design and control of electrical machines, space harmonics, drive systems, and power electronics. In 1995, he joined the Department of Electrical Engineering, Electrics and Electronics Faculty, ITU, where he has been an Assistant Professor, since January 2009.

...